JMEPEG (2012) 21:1120–1132
DOI: 10.1007/s11665-011-0020-3

1059-9495/$19.00

Dielectric Response of High Explosives at THz Frequencies Calculated Using Density Functional Theory

L. Huang, A. Shabaev, S.G. Lambrakos, N. Bernstein, V. Jacobs, D. Finkenstadt, and L. Massa

(Submitted May 13, 2011)

We present in this study calculations of the ground-state resonance structures associated with the high explosives β-HMX, PETN, RDX, TNT1, and TNT2 using density functional theory (DFT). Our objective is the construction of parameterized dielectric-response functions for excitation by electromagnetic waves at compatible frequencies. These dielectric-response functions provide the basis for analyses pertaining to the dielectric properties of explosives. In particular, these dielectric-response functions provide quantitative initial estimates of spectral-response features for subsequent adjustment with knowledge of additional information, such as laboratory measurements and other types of theory-based calculations. With respect to qualitative analyses, these spectra provide for the molecular-level interpretation of response structure. The DFT software GAUSSIAN was used for the calculations of the ground-state resonance structures presented here.

Keywords chemical analysis, material selection, modeling processes

1. Introduction

A significant aspect of using response spectra calculated using density functional theory (DFT) for the direct construction of permittivity functions is that it adopts the perspective of computational physics, according to which a numerical simulation represents another source of ''experimental'' data. This perspective is significant in that a general procedure may be developed for the construction of permittivity functions using DFT calculations as a quantitative initial estimate of spectral-response features for subsequent adjustment with knowledge of additional information, such as experimental measurements and other types of theory-based calculations. In other words, for the purpose of simulating many electromagnetic-response characteristics of materials, DFT is sufficiently mature for the purpose of generating data complementing, as well as superseding, experimental measurements.

In the case of THz excitation of materials, the procedure of using response spectra calculated using DFT for the direct construction of permittivity functions is well defined, owing to the physical characteristic of THz excitation. In particular, it is important to note that the procedure for constructing a permittivity function using response spectra calculated using DFT is physically consistent with the linear response associated with THz excitation of molecules. Accordingly, one observes a correlation between the advantages of using THz excitation for detection of IEDs (and ambient materials) and those for its numerical simulation based on DFT. Specifically, THz excitation is associated with frequencies that are characteristically perturbative to molecular states, in contrast to frequencies that can induce appreciable electronic-state transitions. Of course, the practical aspect of the perturbative character of THz excitation for detection is that detection methodologies can be developed, which do not damage materials under examination. The perturbative character of THz excitation with respect to molecular states has significant implications with respect to its numerical simulation based on DFT. It follows then that, owing to the perturbative character of THz excitation, which is characteristically linear, one is able to make a direct association between local oscillations about the ground-state minima of a given molecule and THz excitation spectra.

In what follows, calculations are presented of the ground-state resonance structure associated with the high explosives β-HMX, PETN, RDX, TNT1, and TNT2 using DFT. This resonant structure is utilized for the construction of parameterized dielectric-response functions for excitation by electromagnetic waves at compatible frequencies. For this purpose, the DFT software GAUSSIAN09 (G09) has been adopted (Ref 1).

The organization of the subject areas presented in this article is as follows. First, a general review of the elements of the vibrational analysis using DFT, which are relevant for the calculation of absorption spectra is presented. Second, a general review is presented concerning the formal structure of permittivity functions in terms of analytic-function representations. An understanding of the formal structure of permittivity functions, in terms of both physical consistency and causality, is important for the post-processing of DFT calculations for the purpose of constructing permittivity functions. Third, information concerning the ground-state resonance structure of the explosives β-HMX, PETN, RDX, TNT1 and TNT2, which is obtained using DFT, is presented as a set of case studies. This

L. Huang, S.G. Lambrakos, N. Bernstein, and **V. Jacobs**, Naval Research Laboratory, Washington, DC 20375; **A. Shabaev**, George Mason University, Fairfax, VA 22030; **D. Finkenstadt**, Physics Department, U.S. Naval Academy, Annapolis, MD 21402; and **L. Massa**, Hunter College, CUNY, New York, NY 10065. Contact e-mail: lambrakos@anvil.nrl.navy.mil.

information consists of the ground-state molecular geometry and the response spectrum for an isolated molecule. In addition, for each of the explosives, a prototype calculation is presented to demonstrate the construction of parameterized permittivity functions using response spectra calculated using DFT.

2. Construction of Permittivity Functions using DFT

2.1 Density Functional Theory

The application of DFT and related methodologies for the determination of electromagnetic-response characteristics is important for the analysis of parameter sensitivity. In other words, many characteristics of the electromagnetic response of a given material may not be detectable, or in general, not relevant for detection. Accordingly, sensitivity analyses concerning the electromagnetic response of layered composite systems can incorporate the results of simulations using DFT, and related methodologies, to provide realistic limits on detectability that are independent of a specific system design for IED detection. In addition, analyses of parameter sensitivity based on the atomistic response characteristics of a given material, obtained by DFT, provide for an "optimal" best fit of experimental measurements for the construction of permittivity functions. It follows that, within the context of parameter sensitivity analyses, the dataset obtained by means of DFT represents a true complement to that obtained by means of experimental measurements.

The DFT software GAUSSIAN09 (G09) can be used for computing an approximation of the IR absorption spectrum of a molecule (Ref 1). This program calculates vibrational frequencies by determining second derivatives of the energy with respect to the Cartesian nuclear coordinates, and then transforms to mass-weighted coordinates at a stationary point of the geometry (Ref 2). The IR absorption spectrum is obtained using Kohn-Sham DFT (Ref 3-7) to compute the ground-state electronic structure in the Born-Oppenheimer approximation. GAUSSIAN uses specified orbital-basis functions to represent the electronic wavefunctions and density. For a given set of nuclear positions, the calculation directly gives the electronic charge density of the molecule, the potential energy V, and the displacements in Cartesian coordinates of each atom. The procedure for the vibrational analysis followed in GAUSSIAN is as described in Ref 8. Reference 9 presents a fairly detailed review of this procedure. A brief description of this procedure is as follows.

The procedure followed by GAUSSIAN is based on the fact the vibrational spectrum depends on the Hessian matrix, $\mathbf{f}_{\mathrm{CART}}$, which is constructed using the second partial derivatives of the potential energy V with respect to displacements of the atoms in Cartesian coordinates. Accordingly, the elements of the $3N \times 3N$ matrix $\mathbf{f}_{\mathrm{CART}}$ are given by

$$f_{\mathrm{CART}_{ij}} = \left(\frac{\partial^2 V}{\partial \xi_i \partial \xi_j}\right)_0 \qquad \text{(Eq 1)}$$

where $\{\xi_1, \xi_2, \xi_3, \xi_4, \xi_5, \xi_6, \ldots, \xi_{3N}\} = \{\Delta x_1, \Delta y_1, \Delta z_1, \Delta x_2, \Delta y_2, \Delta z_2, \ldots, \Delta z_N\}$, which are displacements in Cartesian coordinates, and N is the number of atoms. As discussed above, the zero subscript in Eq 1 indicates that the derivatives are evaluated at the equilibrium positions of the atoms, and that the first derivatives are zero. Given the Hessian matrix defined by Eq 1, the operations for the calculation of the vibrational spectrum require that the Hessian matrix Eq 1 be transformed to mass-weighted Cartesian coordinates according to the relation:

$$f_{\mathrm{MWC}_{ij}} = \frac{f_{\mathrm{CART}_{ij}}}{\sqrt{m_i m_j}} = \left(\frac{\partial^2 V}{\partial q_i \partial q_j}\right)_0 \qquad \text{(Eq 2)}$$

where $\{q_1, q_2, q_3, q_4, q_5, q_6, \ldots, q_{3N}\} = \{\sqrt{m_1}\Delta x_1, \sqrt{m_1}\Delta y_1, \sqrt{m_1}\Delta z_1, \sqrt{m_2}\Delta x_2, \sqrt{m_2}\Delta y_2, \sqrt{m_2}\Delta z_2, \ldots, \sqrt{m_N}\Delta z_N\}$ are the mass-weighted Cartesian coordinates. GAUSSIAN computes the energy second derivatives Eq 2, thus computing the forces for displacement perturbations of each atom along each Cartesian direction. The first derivatives of the dipole moment with respect to the atomic positions $\partial\vec{\mu}/\partial\xi_i$ are also computed. Each vibrational eigenmode leads to a single peak in the absorption spectrum, at a frequency equal to the mode's eigenfrequency ν_{n0}. The absorption intensity corresponding to a particular eigenmode n, whose eigenfrequency is ν_{n0}, is given by

$$I_n = \frac{\pi}{3c}\left|\sum_{i=1}^{3N}\frac{\partial\vec{\mu}}{\partial\xi_i} l_{\mathrm{CART}_{in}}\right|^2, \qquad \text{(Eq 3a)}$$

where $\mathbf{l}_{\mathrm{CART}}$ is the matrix the column vectors of which are the normal modes represented by the displacements of the atoms in Cartesian coordinates, and the normalization constant N_n is given by

$$N_n = \sqrt{\sum_{i=1}^{3N} l^2_{\mathrm{CART}_{in}}} \qquad \text{(Eq 3b)}$$

The matrix $\mathbf{l}_{\mathrm{CART}}$ is determined by the following procedure: First,

$$\mathbf{l}_{\mathrm{CART}} = \mathbf{M}\mathbf{l}_{\mathrm{MWC}} \qquad \text{(Eq 4)}$$

where $\mathbf{l}_{\mathrm{MWC}}$ is the matrix the elements of which are the displacements of the atoms in mass-weighted Cartesian coordinates and $\mathbf{M}$ is a diagonal matrix defined by the elements:

$$M_{ii} = \frac{1}{\sqrt{m_i}} \qquad \text{(Eq 5)}$$

Proceeding, $\mathbf{l}_{\mathrm{MWC}}$ is the matrix needed to diagonalize $\mathbf{f}_{\mathrm{MWC}}$ defined by Eq 2 such that

$$(\mathbf{l}_{\mathrm{MWC}})^{\mathrm{T}}\mathbf{f}_{\mathrm{MWC}}(\mathbf{l}_{\mathrm{MWC}}) = \Lambda, \qquad \text{(Eq 6)}$$

where Λ is the diagonal matrix with eigenvalues λ_i. The superscript "T" in Eq 6 denotes the transpose of the matrix. The procedure for diagonalizing Eq 6 consists of the operations:

$$\mathbf{f}_{\mathrm{INT}} = (\mathbf{D})^{\mathrm{T}}\mathbf{f}_{\mathrm{MWC}}(\mathbf{D}) \qquad \text{(Eq 7)}$$

and

$$(\mathbf{L})^{\mathrm{T}}\mathbf{f}_{\mathrm{INT}}(\mathbf{L}) = \Lambda, \qquad \text{(Eq 8)}$$

where $\mathbf{D}$ is a matrix transformation to coordinates where rotation and translation have been separated out, and $\mathbf{L}$ is the transformation matrix composed of eigenvectors calculated

according to Eq 8. The eigenfrequencies in units of (cm^{-1}) are calculated using the eigenvalues λ_n by means of the expression:

$$\nu_{n0} = \frac{\sqrt{\lambda_n}}{2\pi c}, \quad \text{(Eq 9)}$$

where c is the speed of light. The elements of $\mathbf{l}_{\mathrm{CART}}$ are given by

$$l_{\mathrm{CART}_{in}} = \sum_{j=1}^{3N} \frac{D_{nj} L_{ji}}{\sqrt{m_j}}, \quad \text{(Eq 10)}$$

where n, $i = 1, \ldots, 3N$, and the column vectors of these elements are the normal modes in Cartesian coordinates.

The intensity Eq 3 must then be multiplied by the number density of molecules to give an absorption strength. It follows that the absorption spectrum calculated by GAUSSIAN is a sum of delta functions, the positions and magnitudes of which correspond to the vibrational frequencies and electromagnetic-transition intensitiess, respectively. In principle, however, these spectral components must be broadened and shifted to account for anharmonic effects, such as finite mode lifetimes and inter-mode couplings.

2.2 Dielectric Permittivity Functions

The general approach of constructing permittivity functions according to the best fit of available data for a given material corresponding to many different types of experimental measurements is not unprecedented, and has been typically the dominant approach. Presented in this article is an extension of this approach in that the calculations of electromagnetic response based on DFT are also employed to provide data for the construction of permittivity functions. The inclusion of this type of information is necessary for accessing what spectral response features at the molecular level are actually detectable

Table 1 Atomic positions of β-HMX (Å)

Atomic number	X	Y	Z	Atomic number	X	Y	Z
6	−0.247569	2.398888	−0.24206	8	−0.481761	2.084279	−2.852395
6	−2.063866	0.625101	−0.034283	8	−2.079477	0.60568	−2.657757
6	1.429414	0.449077	−0.072891	8	1.610321	3.877071	0.675548
6	−0.386827	−1.324705	0.135093	8	3.18386	2.364102	0.605726
7	−1.131623	1.421861	−0.823793	8	−2.244633	−2.802996	−0.782467
7	1.122469	1.866827	−0.101235	8	−3.818203	−1.290037	−0.712928
7	0.497123	−0.347527	0.716733	1	−0.643824	2.678988	0.732229
7	−1.756822	−0.79264	−0.00604	1	−0.208649	3.282257	−0.86844
7	0.608684	−0.301254	2.107395	1	−3.075188	0.711052	−0.417038
7	−1.242997	1.375573	−2.214453	1	−2.026551	1.032712	0.973025
7	2.039759	2.752548	0.444065	1	0.009539	−1.605043	−0.839084
7	−2.674091	−1.678436	−0.551159	1	−0.425827	−2.207929	0.761672
8	−0.152503	−1.009914	2.74544	1	2.440755	0.363063	0.309801
8	1.445216	0.468641	2.550583	1	1.392	0.0414	−1.080169

Table 2 Oscillation frequencies and IR intensities of β-HMX

Frequency, cm^{-1}	Intensity, km/mol	Frequency, cm^{-1}	Intensity, km/mol	Frequency, cm^{-1}	Intensity, km/mol	Frequency, cm^{-1}	Intensity, km/mol
20.5974	4.4642	423.5457	0.0001	958.1357	275.8733	1439.7352	12.4616
46.5227	6.2401	424.4072	6.6649	958.7657	0.0321	1455.7355	0
59.4169	0	595.4743	0	1078.5529	0.0015	1479.3719	0.0002
64.9626	2.6874	598.3283	38.8195	1084.0758	134.3721	1480.1064	48.3128
65.5097	0.0005	628.1299	32.6053	1154.6108	191.9206	1494.9257	0
91.0091	0	632.9158	0	1192.3604	0	1499.1006	95.5194
95.7746	0.4885	653.1038	5.7687	1219.5098	0	1597.9156	0.012
116.2327	0	655.3446	0	1233.8676	170.6558	1603.1827	654.1091
123.5112	0.5691	733.673	0	1261.0272	96.8792	1615.2202	0.024
155.7534	0	763.9167	13.9813	1261.6361	0.01	1617.4993	690.7993
165.5881	10.9519	769.637	0	1288.3562	0.0001	3080.0298	0.0009
202.3398	20.9064	776.5606	20.6047	1296.1097	977.5485	3081.1194	9.6204
220.1601	0	776.9724	0.0013	1310.3824	472.4158	3098.6262	25.9659
273.6165	0	783.8961	20.1101	1338.5525	0	3098.9294	0.0053
296.5221	0	839.4502	0.0003	1338.9509	0	3158.0271	0.0172
340.787	7.1838	840.1406	5.2862	1352.0732	20.0148	3158.1956	11.0469
344.5913	0	877.9347	15.0169	1374.7476	0.1501	3161.4685	4.0618
377.1029	6.4205	888.8403	0	1374.8451	17.9345	3161.7092	0.002
400.4941	0.0002	942.4828	289.7913	1404.5298	0		
402.1082	5.773	947.8026	0.0006	1426.7612	47.7131		

with respect to a given set of detection parameters. Accordingly, permittivity functions, having been constructed using DFT calculations, can provide a quantitative correlation between macroscopic material response and molecular structure, where the macroscopic system can in general consist of either uncoupled or coupled molecules. Within this context, for the purpose of being adopted for system simulation, it is not necessary that the permittivity function be precisely determined. Rather, it is only necessary that the permittivity function be qualitatively represented, in terms of specific dielectric-response features that play an important role in sensitivity analyses, which are relevant for the assessment of the absolute delectability of different types of molecular structures with respect to a given set of detection parameters. In other words, permittivity functions that have been determined using DFT can provide a mechanistic interpretation of material response to electromagnetic excitation, which could establish the applicability of a given detection methodology for the detection of specific molecular characteristics. Within the context of practical applications to the proper interpretation of permittivity-function features, permittivity functions having been constructed according to the best fit of available data would be "correlated" with those obtained using DFT. Subsequent to the establishment of good correlation between DFT calculations

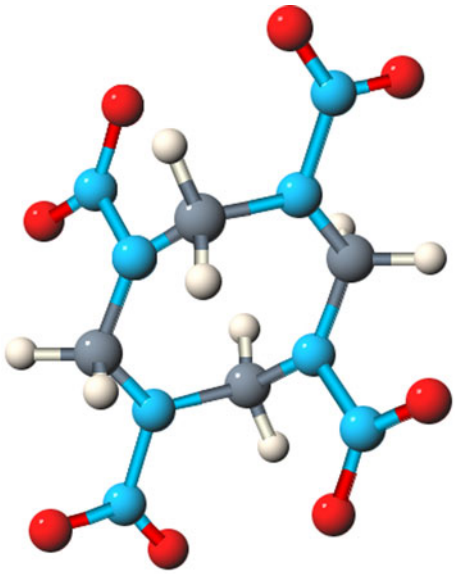

Fig. 1 Molecular geometry of β-HMX

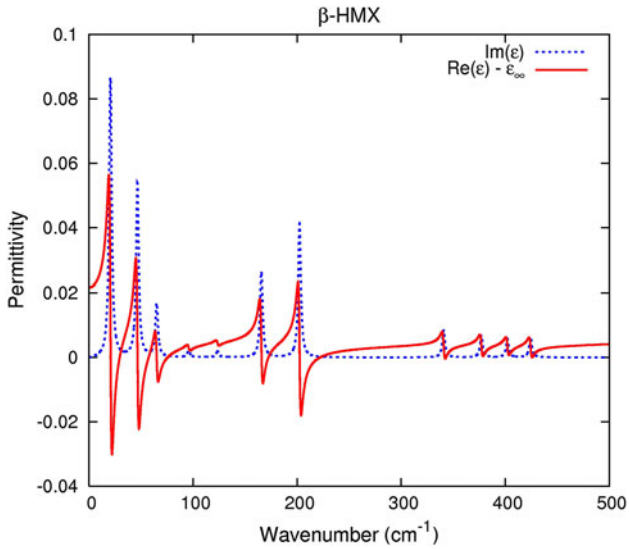

Fig. 3 Real (solid) and imaginary (dashed) parts of permittivity function of β-HMX molecules with $\gamma_n = 3\ \mathrm{cm}^{-1}$ and $\rho = 2.4 \times 10^{19}\ \mathrm{cm}^{-3}$ for frequencies within THz range

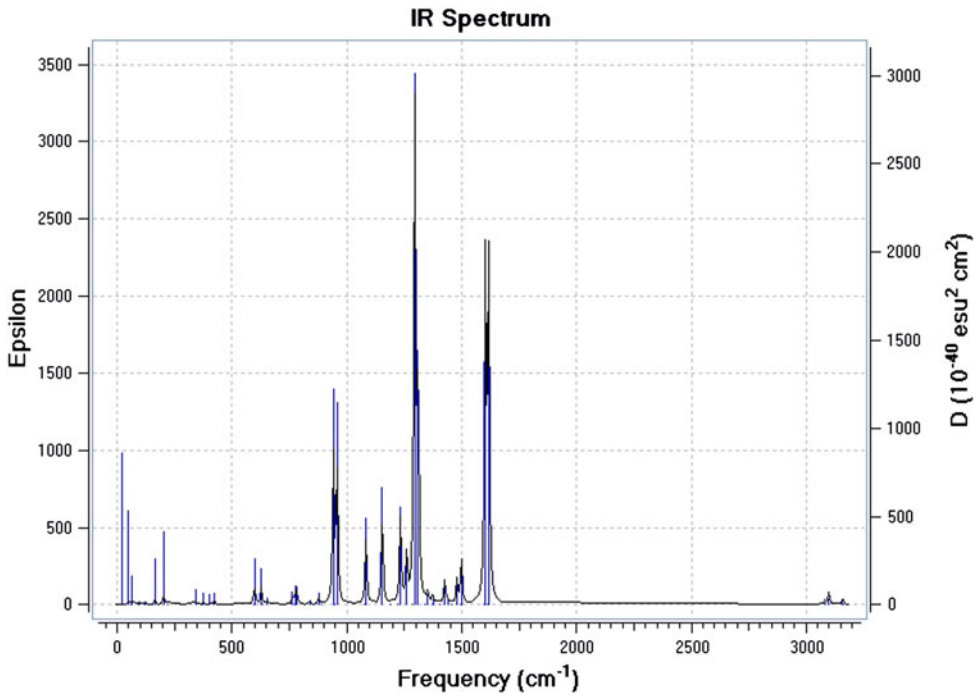

Fig. 2 IR intensity as a function of frequency calculated using DFT B3LYP/6-311++G(2d,2p) for β-HMX according to frozen-phonon approximation

Table 3 Atomic positions of PETN (Å)

Atomic number	*X*	*Y*	*Z*	Atomic number	*X*	*Y*	*Z*
6	−0.89008	0.487044	0.169443	8	1.885603	−3.148164	−0.06536
6	0.56833	0.025631	0.355901	8	2.801652	−1.246607	0.487954
6	−0.954153	2.010353	0.393203	1	−1.969444	2.373078	0.253141
6	−1.775405	−0.266852	1.180709	1	−0.289344	2.531375	−0.29121
6	−1.399001	0.17896	−1.25209	1	0.903906	0.201954	1.374781
8	−0.536524	2.246621	1.753563	1	1.224466	0.550575	−0.333979
8	0.594489	−1.388358	0.071682	1	−1.43301	−0.084138	2.196278
8	−3.114945	0.243543	1.019535	1	−1.763653	−1.336176	0.985073
8	−0.503707	0.845656	−2.165744	1	−2.410743	0.55161	−1.391197
8	−5.169236	0.102355	1.756224	1	−1.382201	−0.89204	−1.438315
8	−3.660475	−1.176108	2.678384	7	−4.069163	−0.341502	1.911776
8	−0.213539	3.790051	3.268901	7	−0.561634	3.625752	2.13612
8	−0.916392	4.418249	1.301021	7	1.895046	−1.976796	0.177844
8	−0.065066	1.202636	−4.278301	7	−0.825239	0.640236	−3.54537
8	−1.784867	−0.046988	−3.786458				

Table 4 Oscillation frequencies and IR intensities of PETN

Frequency, cm^{-1}	Intensity, km/mol	Frequency, cm^{-1}	Intensity, km/mol	Frequency, cm^{-1}	Intensity, km/mol	Frequency, cm^{-1}	Intensity, km/mol
24.1944	2.0809	316.0741	0	923.26	9.1634	1410.9082	32.0286
25.1486	0.0001	449.6382	3.5611	945.7603	8.2868	1422.7894	0.0001
39.6217	0.1006	449.678	3.56	945.7964	8.3144	1514.4496	0
40.7946	1.0765	531.1423	17.475	1009.2443	0.0001	1515.8597	6.4408
40.8093	1.078	586.0232	0	1018.9313	69.2683	1519.5519	17.4451
48.8877	0	616.7118	12.0616	1018.9486	69.3583	1519.5752	17.4574
50.6657	0.0052	621.5385	11.9061	1057.7988	110.9231	1704.4698	0.0468
55.4863	1.7452	621.5649	11.9235	1061.3842	0	1706.0529	293.7907
55.508	1.7454	671.4305	0	1182.1622	2.0461	1707.5656	669.1497
124.2462	0.5941	707.5737	66.0545	1201.7557	0.075	1707.6	669.3272
124.2875	0.594	707.6072	66.0823	1201.7788	0.0741	3085.7715	7.5588
132.7604	1.1955	754.7934	71.5529	1270.1554	0.0002	3086.3389	5.5306
145.448	0	769.8139	11.3843	1288.5605	44.1673	3086.384	5.5486
172.1583	0	769.8161	11.352	1288.6211	44.2379	3088.3333	0.0006
190.9592	1.002	770.3806	0.0003	1303.6309	425.1637	3139.4114	0.0009
191.0142	1.0007	771.5349	33.3462	1311.3896	290.9257	3141.219	4.1267
208.874	0	839.1219	0	1311.4103	291.0257	3141.3005	4.1112
248.6994	1.8583	847.8259	385.5923	1325.2662	0.0001	3143.2476	6.39
250.9887	1.5616	847.8293	385.3134	1334.1466	80.9233		
251.031	1.5589	851.4825	768.282	1406.0359	21.6309		
306.1457	1.222	879.0186	0.0002	1406.0658	21.5905		

and experimental measurements, DFT calculations can be adopted as constraints for the purpose of constructing permittivity functions, whose features would be consistent with molecular-level response. This would facilitate the subsequent adjustment following knowledge of specific sets of either experimental data or additional molecular-level information. It should be noted that, among the first studies using DFT calculations to construct permittivity functions was that of Hooper et al. (Ref 10). The permittivity function that was constructed, which was for a periodic lattice of β-HMX molecules, showed good agreement with experimental measurements.

The construction of permittivity functions using DFT calculations involves, however, an aspect that requires serious consideration. This aspect concerns the fact that a specific parametric-function representation must be adopted. Accordingly, any parametric representation, i.e., parameterization, adopted for permittivity-function construction must be physically consistent with specific molecular-response characteristics, while limiting the inclusion of feature characteristics that tend to mask response signatures that may be potentially detectable.

In principle, parameterizations are of two classes. One class consists of parameterizations that are directly related to molecular-response characteristics. This class of parameterizations would include spectral scaling and width coefficients. The other class consists of parameterizations that are purely phenomenological and are structured for optimal and convenient best fits to experimental measurements. A sufficiently general parameterization of permittivity functions is given by the Drude-Lorentz approximation (Ref 11)

$$\varepsilon(\nu) = \varepsilon_r(\nu) + i\varepsilon_i(\nu) = \varepsilon_\infty + \sum_{n=1}^{N} \frac{\nu_{np}^2}{(\nu_{n0}^2 - \nu^2) - i\gamma_n \nu}, \qquad \text{(Eq 11)}$$

where ν_{np} and γ_n are, respectively, the spectral scaling and width of a resonance contributing to the permittivity function. The permittivity ε_∞ is a constant, since the dielectric response at high frequencies is substantially detuned from the probe frequency. The real and imaginary parts, $\varepsilon_r(\nu)$ and $\varepsilon_i(\nu)$, respectively, of the permittivity function can be written separately as

$$\varepsilon_r(\nu) = \varepsilon_\infty + \sum_{n=1}^{N} \frac{\nu_{np}^2(\nu_{n0}^2 - \nu^2)}{(\nu_{n0}^2 - \nu^2)^2 + \gamma_n^2 \nu^2} \qquad \text{(Eq 12)}$$

$$\text{and} \quad \varepsilon_i(\nu) = \sum_{n=1}^{N} \frac{\nu_{np}^2 \gamma_n \nu}{(\nu_{n0}^2 - \nu^2)^2 + \gamma_n^2 \nu^2}$$

With respect to practical application, the absorption coefficient α and index of refraction n_r, given by

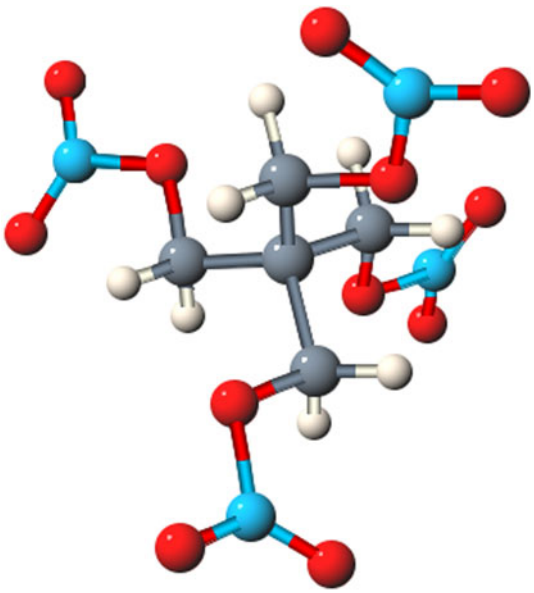

Fig. 4 Molecular geometry of PETN

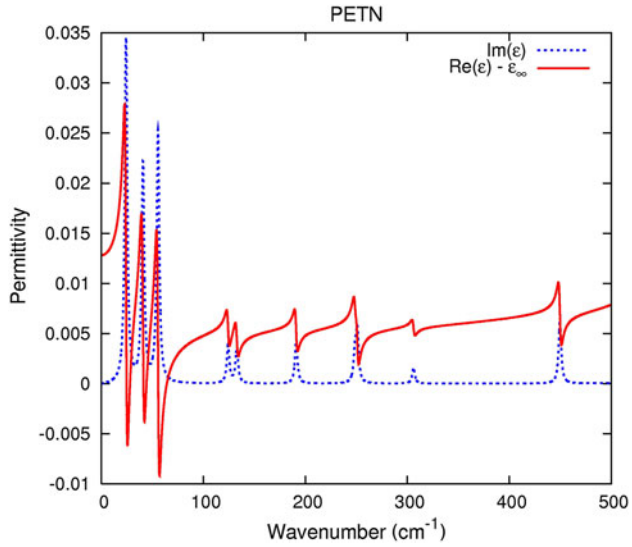

Fig. 6 Real (solid) and imaginary (dashed) parts of permittivity function of PETN molecules with $\gamma_n = 3\ \text{cm}^{-1}$ and $\rho = 2.4 \times 10^{19}\ \text{cm}^{-3}$ for frequencies within THz range

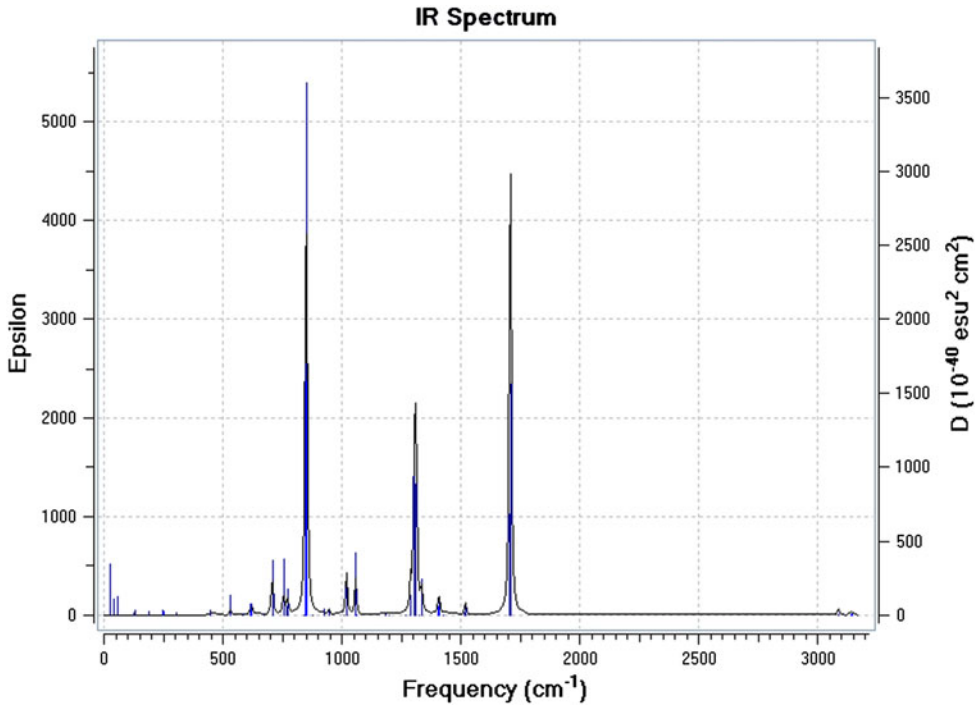

Fig. 5 IR intensity as a function of frequency calculated using DFT B3LYP/6-311++G(2d,2p) for PETN according to frozen-phonon approximation

Table 5 Atomic positions of RDX (Å)

Atomic number	X	Y	Z	Atomic number	X	Y	Z
7	1.177132	−0.800831	0.102459	8	−1.148702	1.861918	2.523892
7	0.102459	1.177132	−0.800831	8	3.333613	−0.184585	0.086238
7	−0.800831	0.102459	1.177132	8	0.086238	3.333613	−0.184585
7	2.436639	−0.679768	0.742611	8	−0.184585	0.086238	3.333613
7	0.742611	2.436639	−0.679768	1	−1.515435	1.871323	0.32473
7	−0.679768	0.742611	2.436639	1	0.32473	−1.515435	1.871323
6	−1.083455	0.93108	0.011066	1	1.871323	0.32473	−1.515435
6	0.011066	−1.083455	0.93108	1	−1.794386	0.385919	−0.609699
6	0.93108	0.011066	−1.083455	1	−0.609699	−1.794386	0.385919
8	2.523892	−1.148702	1.861918	1	0.385919	−0.609699	−1.794386
8	1.861918	2.523892	−1.148702				

Table 6 Oscillation frequencies and IR intensities of RDX

Frequency, cm^{-1}	Intensity, km/mol	Frequency, cm^{-1}	Intensity, km/mol	Frequency, cm^{-1}	Intensity, km/mol	Frequency, cm^{-1}	Intensity, km/mol
36.3016	0.0457	589.5756	12.0529	1008.1423	52.0064	1466.3945	29.2759
36.3016	0.0455	589.5756	12.0501	1008.1423	52.0228	1466.3945	29.2705
65.6946	0.2773	593.3556	0.0005	1137.1893	0.0007	1484.9159	77.5386
66.7914	0.7854	660.3034	3.91	1246.0972	19.5343	1605.9512	0.0006
100.3213	0.0217	660.3034	3.9149	1247.9865	60.5211	1637.2725	455.8935
100.3213	0.0216	755.2321	0.2018	1247.9865	60.5168	1637.2725	455.9394
219.7949	5.4286	764.2693	0.1606	1278.0071	0	3070.623	0.8397
219.7949	5.4314	764.2693	0.161	1289.4368	183.7337	3070.623	0.8394
303.525	0.0004	785.2931	90.7195	1289.4368	183.787	3076.4897	37.061
362.7641	0.2746	859.1682	0.2644	1342.053	338.9161	3201.8977	14.7538
362.7641	0.2747	859.1682	0.2644	1368.4448	0.0158	3201.8977	14.7445
407.6598	0.7931	887.6022	25.785	1385.4041	3.3489	3204.033	16.1921
407.6598	0.7951	909.5884	292.0052	1385.4041	3.3494		
437.1534	11.3308	909.5884	291.9845	1407.8136	17.1052		
457.0457	21.8362	938.4995	118.3704	1407.8136	17.1032		

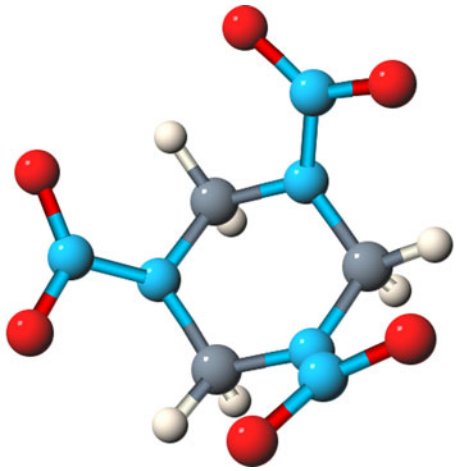

Fig. 7 Molecular geometry of RDX

$$\alpha = \frac{4\pi\nu}{\sqrt{2}}\left[-\varepsilon_r + \sqrt{\varepsilon_r^2 + \varepsilon_i^2}\right]^{1/2}$$

$$\text{and} \quad n_r = \frac{1}{\sqrt{2}}\left[\varepsilon_r + \sqrt{\varepsilon_r^2 + \varepsilon_i^2}\right]^{1/2} \qquad \text{(Eq 13)}$$

respectively, provide direct relationships between calculated quantities obtained using DFT and the "conveniently measurable" quantities, α and n_r. Before proceeding with the more formal development of the physical foundation of Eq 11, it is important to note that the sum given in this expression is over independent oscillators which scatter the incident electromagnetic wave. These oscillators are assumed to be weakly coupled, such that each oscillator responds independently. The ensemble of oscillators, however, is coherently driven by the incident wave which controls the phase of the response contributed by each individual oscillator, thus collectively contributing to the outgoing wave. In our treatment of a system of molecules in gas phase, the normal modes of each molecule are assumed to be those of an isolated structure. We again emphasize that DFT-calculated spectra may be considered the results of computational experiments and that, accordingly, these spectra can be represented by any analytic functional forms, e.g., Drude-Lorentz model, satisfying the Kramers-Kronig relations (Ref 12). It is interesting, however, to note that in fact the form of the Drude-Lorentz model is physically consistent with the structure of DFT-calculated vibrational spectra and that, accordingly, different quantities associated with this model can be interpreted with respect to quantum and statistical-mechanical concepts. Further discussion concerning this point can be found in (Ref 13).

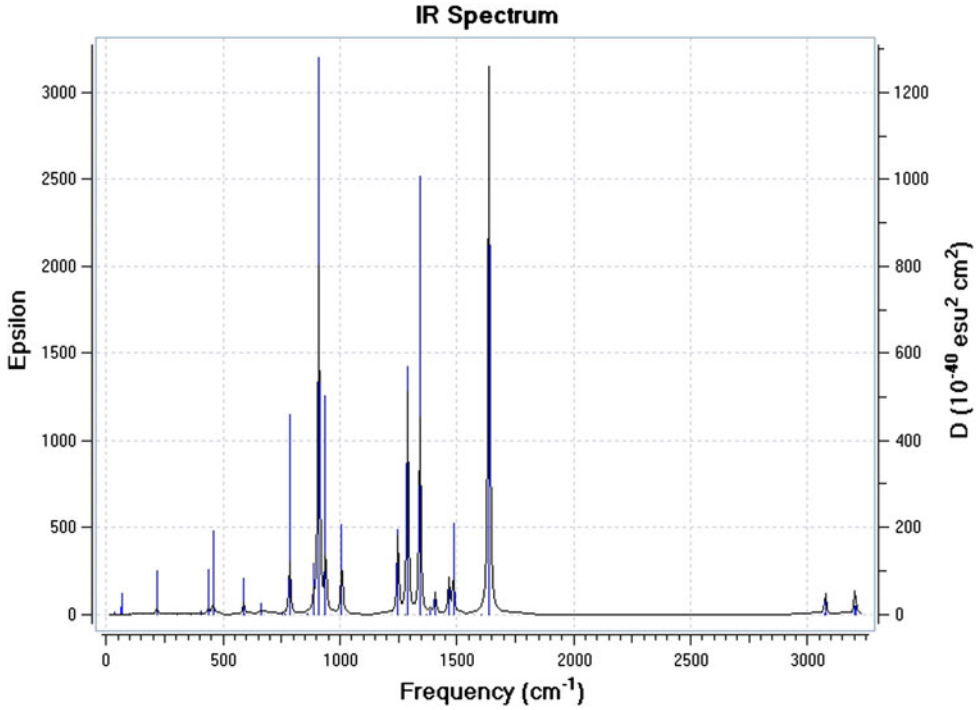

Fig. 8 IR intensity as a function of frequency calculated using DFT B3LYP/6-311++G(2d,2p) for RDX according to frozen-phonon approximation

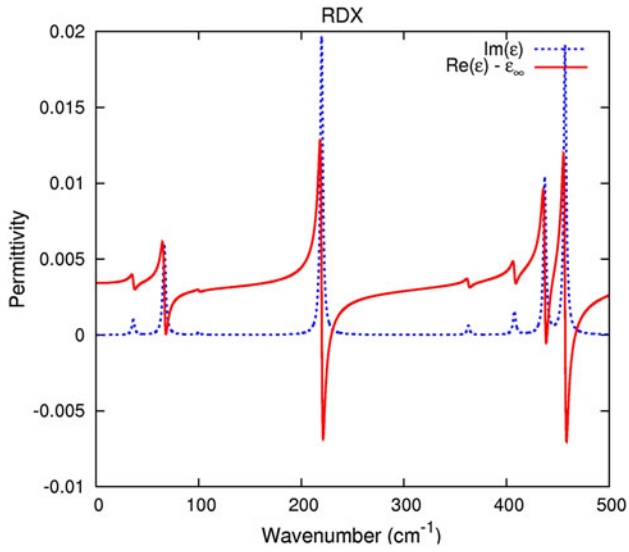

Fig. 9 Real (solid) and imaginary (dashed) parts of permittivity function of RDX molecules with $\gamma_n = 3\ \text{cm}^{-1}$ and $\rho = 2.4 \times 10^{19}\ \text{cm}^{-3}$ for frequencies within THz range

3. Case Study 1: Ground-State Resonance Structure of β-HMX

In this section are presented two sets of data, which are the results of computational experiments using DFT, concerning the molecule β-HMX. These are the relaxed or equilibrium configuration of a single isolated molecule of β-HMX (see Table 1) and ground-state oscillation frequencies and IR intensities for this configuration that are calculated using DFT, according to the frozen-phonon approximation (see Table 2). For these calculations, the geometry optimization and the vibrational analysis were implemented using the DFT model B3LYP (Ref 14, 15) and basis function 6-311++G(2d,2p) (Ref 16). The symbol "++" designates the 6-311G basis-function set supplemented by diffuse functions (Ref 17), and (2d,2p) designates polarization functions having two sets of d functions for heavy atoms and two sets of p functions for hydrogen atoms (Ref 18). A schematic representation of the molecular geometry of β-HMX is shown in Fig. 1. Figure 2 is the IR intensity as a function of frequency for β-HMX, according to a frozen-phonon approximation. For the spectrum shown in Fig. 2, the structure of each resonance response is approximated essentially by that of a delta function.

Next, a permittivity function is constructed using the DFT calculations of GAUSSIAN and the parametric-function representation defined by Eq 11 and 12. Accordingly, shown in Fig. 3 are the real and imaginary parts of a permittivity function corresponding to the electromagnetic response of HMX molecules to excitation within the THz range of frequencies, where the widths of the molecular resonances and the density of molecules are chosen at the following values: $\gamma_n = 3\ \text{cm}^{-1}$ and $\rho = 2.4 \times 10^{19}\ \text{cm}^{-3}$.

4. Case Study 2: Ground-State Resonance Structure of PETN

In this section are presented two sets of data, which are the results of computational experiments using DFT, concerning the molecule PETN. These are the relaxed or equilibrium

Table 7 Atomic positions of TNT1 (Å)

Atomic number	*X*	*Y*	*Z*	Atomic number	*X*	*Y*	*Z*
1	1.294359	−0.627693	1.916458	6	1.399735	−0.432944	−2.779328
1	−2.458208	−0.867791	−0.128619	7	−1.347001	−0.883583	2.313715
1	0.754635	0.052629	−3.504585	7	2.841751	−0.500544	−0.177322
1	1.68668	−1.400164	−3.189867	7	−1.547799	−0.781608	−2.569596
1	2.304987	0.153675	−2.659394	8	3.474661	−1.155138	−0.992685
6	0.730091	−0.664364	0.998736	8	3.321537	0.203741	0.698298
6	−0.646569	−0.782893	1.016672	8	−0.658543	−0.86075	3.323182
6	−1.382696	−0.799534	−0.152696	8	−2.564711	−0.982781	2.284321
6	−0.701136	−0.724375	−1.355556	8	−2.607727	−0.174823	−2.533999
6	0.693755	−0.609698	−1.463028	8	−1.14092	−1.451907	−3.507164
6	1.364308	−0.592195	−0.229936				

Table 8 Oscillation frequencies and IR intensities of TNT1

Frequency, cm^{-1}	Intensity, km/mol	Frequency, cm^{-1}	Intensity, km/mol	Frequency, cm^{-1}	Intensity, km/mol	Frequency, cm^{-1}	Intensity, km/mol
43.8966	0.4182	468.0219	1.6456	955.9036	1.6191	1482.4453	7.5838
46.6024	0.0047	475.7409	0.1431	956.8704	12.4671	1502.2843	9.9084
51.1211	0.3465	538.8592	2.232	1050.7593	1.5785	1577.2756	222.6215
91.7581	5.6023	545.7044	2.7367	1056.2278	1.0227	1585.705	7.1251
116.369	4.314	656.0195	8.947	1097.7349	49.9934	1589.2693	403.4066
148.7023	2.786	668.7824	0.041	1183.8999	11.0977	1637.5889	101.4945
176.8952	0.7688	717.5582	19.2697	1216.2209	0.5961	1645.7786	95.2222
181.9206	0.0608	736.9124	51.5331	1222.8699	12.71	3073.4741	1.3805
182.8245	5.2877	755.0063	29.2922	1337.1632	1.8692	3133.1826	4.432
285.2091	3.1967	788.6055	0.2151	1367.5665	355.2155	3158.8633	4.1296
313.9959	0.301	792.709	3.0718	1377.3833	310.4697	3242.5811	15.8411
319.6074	0.2845	806.3562	13.7704	1386.6946	1.9108	3242.615	29.3568
353.2167	2.4823	839.2241	2.1683	1423.3486	7.5033		
357.4319	2.2329	916.6206	28.8523	1426.8933	9.487		
374.6578	0.1843	945.1449	33.0434	1476.3379	8.1678		

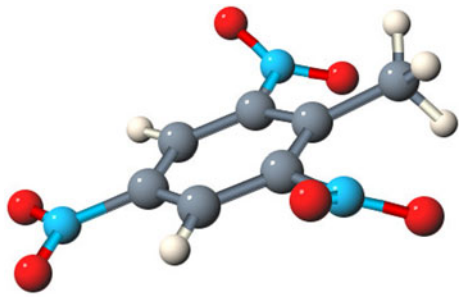

Fig. 10 Molecular geometry of TNT1

configuration of a single isolated molecule of PETN (see Table 3) and ground-state oscillation frequencies and IR intensities for this configuration that are calculated by DFT according to the frozen-phonon approximation (see Table 4). The DFT model and basis-function set used for these calculations are the same as those used in case study 1. A schematic representation of the molecular geometry of PETN is shown in Fig. 4. Figure 5 is the IR intensity as a function of frequency calculated using DFT for PETN, according to a frozen-phonon approximation. For the spectrum shown in Fig. 5, the structure of each resonance response is approximated essentially by that of a delta function.

Next, a permittivity function is constructed using the DFT calculations of GAUSSIAN and the parametric-function representation defined by Eq 11 and 12. Accordingly, shown in Fig. 6 are the real and imaginary parts of a permittivity function corresponding to the electromagnetic response of β-HMX molecules to excitation within the THz range of frequencies, where the widths of the molecular resonances and the density of molecules are chosen at the following values: $\gamma_n = 3\,\mathrm{cm}^{-1}$ and $\rho = 2.4 \times 10^{19}\,\mathrm{cm}^{-3}$.

5. Case Study 3: Ground-State Resonance Structure of RDX

In this section are presented two sets of data, which are the results of computational experiments using DFT, concerning the molecule RDX. These are the relaxed or equilibrium configuration of a single isolated molecule of RDX (see Table 5) and ground-state oscillation frequencies and IR intensities for this configuration that are calculated using DFT according to the frozen-phonon approximation (see Table 6). The DFT model and basis-function set used for these calculations are the same as those used in case study 1. A schematic representation of the molecular geometry of RDX is shown in Fig. 7. Shown in the figure is the IR intensity as a function of frequency calculated using DFT for RDX according to a

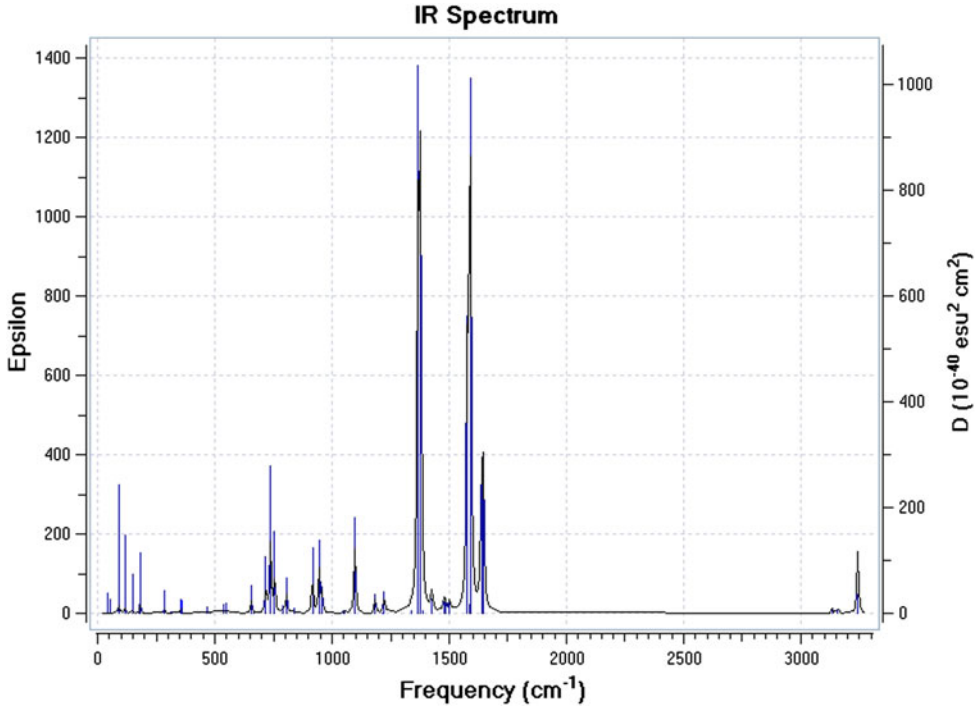

Fig. 11 IR intensity as a function of frequency calculated using DFT B3LYP/6-311++G(2d,2p) for TNT1 according to frozen-phonon approximation

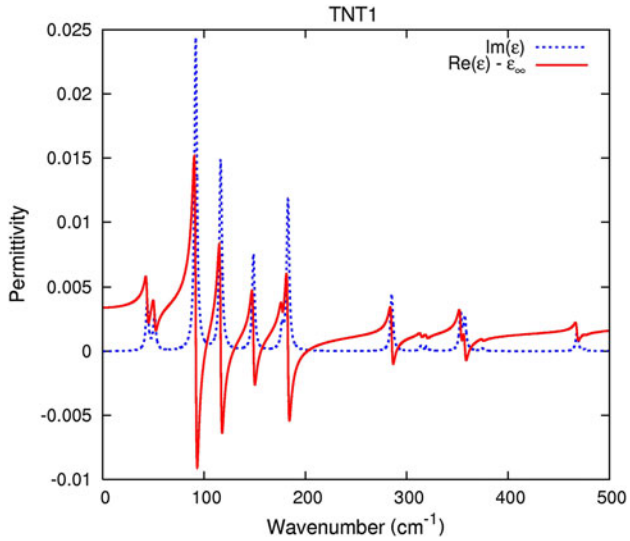

Fig. 12 Real (solid) and imaginary (dashed) parts of permittivity function of TNT1 molecules with $\gamma_n = 3\ \mathrm{cm}^{-1}$ and $\rho = 2.4 \times 10^{19}\ \mathrm{cm}^{-3}$ for frequencies within THz range

frozen-phonon approximation. For the spectrum shown in Fig. 8, the structure of each resonance response is approximated essentially by that of a delta function.

Next, a permittivity function is constructed using the DFT calculations of GAUSSIAN and the parametric-function representation defined by Eq 11 and 12. Accordingly, shown in Fig. 9 are the real and imaginary parts of a permittivity function corresponding to the electromagnetic response of β-HMX molecules to excitation within the THz range of frequencies, where the widths of the molecular resonances and the density of molecules are chosen at the following values: $\gamma_n = 3\ \mathrm{cm}^{-1}$ and $\rho = 2.4 \times 10^{19}\ \mathrm{cm}^{-3}$.

6. Case Study 4: Ground-State Resonance Structure of TNT1

In this section are presented two sets of data, which are the results of computational experiments using DFT, concerning the molecule TNT1. These are the relaxed or equilibrium configuration of a single isolated molecule of TNT1 (see Table 7) and ground-state oscillation frequencies and IR intensities for this configuration that are calculated by DFT according to the frozen-phonon approximation (see Table 8). The DFT model and basis-function set used for these calculations are the same as those used in case study 1. A schematic representation of the molecular geometry of TNT1 is shown in Fig. 10. Figure 11 is the IR intensity as a function of frequency calculated using DFT for TNT1, according to a frozen-phonon approximation. For the spectrum shown in Fig. 11, the structure of each resonance response is approximated essentially by that of a delta function.

Next, a permittivity function is constructed using the DFT calculations of GAUSSIAN and the parametric-function representation defined by Eq 11 and 12. Accordingly, shown in Fig. 12 are the real and imaginary parts of a permittivity function corresponding to the electromagnetic response of β-HMX molecules to excitation within the THz range of frequencies, where the widths of the molecular resonances and the density of molecules are chosen at the following values: $\gamma_n = 3\ \mathrm{cm}^{-1}$ and $\rho = 2.4 \times 10^{19}\ \mathrm{cm}^{-3}$.

Table 9 Atomic positions of TNT2 (Å)

Atomic number	*X*	*Y*	*Z*	Atomic number	*X*	*Y*	*Z*
1	1.272638	−0.725622	1.937201	6	1.414562	−0.48061	−2.757522
1	−2.47618	−0.756181	−0.127018	7	−1.38262	−0.826509	2.318558
1	0.783524	−0.783344	−3.582949	7	2.827982	−0.47615	−0.137647
1	2.308659	−1.100179	−2.762622	7	−1.555219	−0.729874	−2.559208
1	1.745243	0.546032	−2.910146	8	3.370156	0.303405	−0.907211
6	0.710963	−0.694766	1.017803	8	3.395655	−1.156863	0.702976
6	−0.669911	−0.747063	1.027129	8	−0.702058	−0.818858	3.333474
6	−1.398471	−0.726939	−0.147069	8	−2.602448	−0.894081	2.279716
6	−0.705392	−0.681604	−1.344792	8	−2.471574	0.074847	−2.615511
6	0.690578	−0.591628	−1.44343	8	−1.301622	−1.585811	−3.393552
6	1.352575	−0.590481	−0.204408				

Table 10 Oscillation frequencies and IR intensities of TNT2

Frequency, cm^{-1}	Intensity, km/mol	Frequency, cm^{-1}	Intensity, km/mol	Frequency, cm^{-1}	Intensity, km/mol	Frequency, cm^{-1}	Intensity, km/mol
42.0597	0.5991	411.8908	0.9361	952.4309	12.6243	1486.6581	6.208
46.8624	0.0008	504.5207	4.3108	955.8323	4.7116	1511.8199	17.3952
54.1237	0.175	542.3399	2.6744	1046.9528	2.0737	1577.0751	203.8374
73.6054	4.3526	580.5687	0.4432	1062.375	3.8168	1587.4009	280.5907
112.748	4.0026	597.2664	0.2412	1099.163	45.3744	1591.2745	207.5624
145.2265	1.5182	691.0656	23.9547	1184.0508	13.0568	1636.2683	98.2833
151.6023	2.6227	722.2813	4.3961	1216.8298	0.1771	1644.4102	52.6965
176.271	4.5499	737.6184	52.5565	1225.9679	11.4654	3071.1985	0.2464
179.9933	0.2715	763.4611	24.2778	1333.5236	1.7359	3120.1721	2.3101
278.5363	2.7931	774.787	5.025	1367.8151	356.8663	3186.2969	3.0995
308.1643	0.9928	798.3304	0.8215	1379.8845	270.1632	3238.0894	19.668
316.5652	0.4201	805.6322	13.5669	1392.578	42.5101	3243.6443	22.7845
349.3323	1.3951	839.0777	2.2141	1421.7412	11.0304		
354.8972	2.8862	915.717	30.5435	1428.6144	9.6139		
392.2231	2.6389	944.7272	29.7742	1474.3002	0.6607		

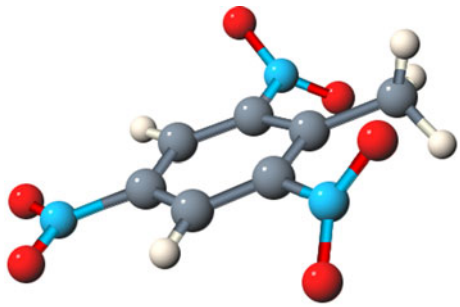

Fig. 13 Molecular geometry of TNT2

7. Case Study 5: Ground-State Resonance Structure of TNT2

In this section are presented two sets of data, which are the results of computational experiments using DFT, concerning the molecule TNT2. These are the relaxed or equilibrium configuration of a single isolated molecule of TNT2 (see Table 9) and ground-state oscillation frequencies and IR intensities for this configuration that are calculated by DFT, according to the frozen-phonon approximation (see Table 10). The DFT model and basis-function representation used for these calculations are the same as those used in case study 1. A schematic representation of the molecular geometry of TNT2 is shown in Fig. 13. Figure 14 is the IR intensity as a function of frequency calculated using DFT for TNT2, according to a frozen-phonon approximation. For the spectrum shown in Fig. 14, the structure of each resonance response is approximated essentially by that of a delta function.

Next, a permittivity function is constructed using the DFT calculations of GAUSSIAN and the parametric-function representation defined by Eq 11 and 12. Accordingly, shown in Fig. 15 are the real and imaginary parts of a permittivity function corresponding to the electromagnetic response of β-HMX molecules to excitation within the THz range of frequencies, where the widths of the molecular resonances and the density of molecules are chosen at the following values: $\gamma_n = 3\,\mathrm{cm}^{-1}$ and $\rho = 2.4 \times 10^{19}\,\mathrm{cm}^{-3}$.

8. Discussion

The DFT-calculated absorption spectra given in Tables 2, 4, 6, and 8 provide two types of information for general analyses of dielectric response. These are the denumeration of ground-state resonance modes, and the estimates of molecular-level dielectric-response structure. The construction of permittivity functions using the DFT-calculated absorption spectra follows the same procedure as that applied for the construction of

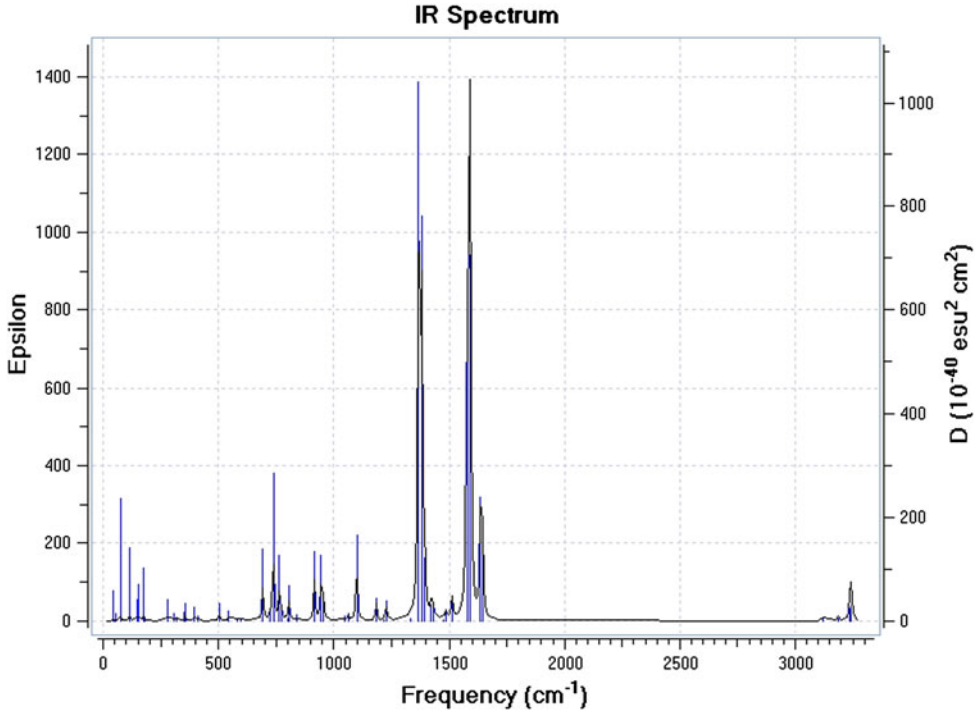

Fig. 14 IR intensity as a function of frequency calculated using DFT B3LYP/6-311++G(2d,2p) for TNT2 according to frozen-phonon approximation

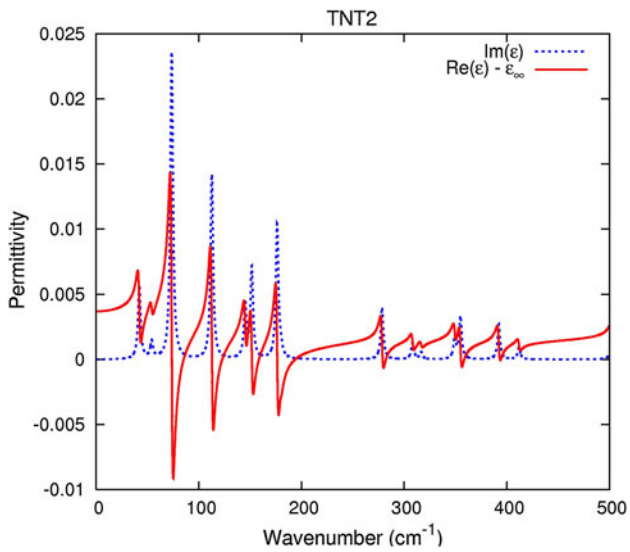

Fig. 15 Real (solid) and imaginary (dashed) parts of permittivity function of TNT2 molecules with $\gamma_n = 3\ \mathrm{cm}^{-1}$ and $\rho = 2.4 \times 10^{19}\ \mathrm{cm}^{-3}$ for frequencies within THz range

permittivity functions using experimentally measured absorption spectra, but with the addition of certain constraint conditions. Accordingly, construction of permittivity functions using either DFT or experimentally measured absorption spectra requires parameterizations that are in terms of physically consistent analytic-function representations, such as the Drude-Lorentz model. Although the formal structure of permittivity functions constructed using DFT and experimental measurements are the same, their interpretation with respect to parameterization is different for each case.

The construction of permittivity functions using experimental measurements defines an inverse problem where resonant locations, peaks, and widths, as well as the number of resonances, are assumed adjustable. Based on this approach, it follows that many of the detailed characteristics of resonance structure are smoothed or averaged. In addition, measurement artifacts associated with sample preparation and detector configuration can in principle introduce errors. One advantage of permittivity functions constructed using experimental measurements, however, is that many aspects of dielectric response on the macroscale, which are associated with multiscale averaging and molecule-lattice coupling, are taken into account inherently. Accordingly, the disadvantage of this approach is that the nature of any multiscale averaging and resonant structure, contributing to dielectric response on the macroscopic level, may not be fully understood. This lack of quantitative understanding can in principle inhibit the development of pump-probe type methodologies for selective excitation of molecular modes, which are intended for the purpose of enhanced signature detection or modulation.

The construction of permittivity functions using DFT calculations, the methodology development of which is considered in this case, defines a direct problem approach where dielectric response is estimated within the bounds of relatively well-defined adjustable parameters. Based on this approach, a permittivity function is constructed using the DFT-calculated absorption spectra, e.g., Tables 2, 4, 6, 8, and 10, under the condition that the calculated resonance locations are fixed, while resonance widths and number densities are assumed adjustable, e.g., Fig. 3, 6, 9, 12, and 15. Better interpretation of dielectric response of explosives on a macroscale can be achieved through correlation of the resonance structure that is experimentally observed and calculated using DFT. In principle, correlation of resonance structure would include the

quantitative analysis of changes in the signature features associated with the transition of the system from that of a low-density system of uncoupled molecule to that of a bulk lattice.

With respect to spectroscopic methods for the detection of explosives, i.e., different types of detection strategies and their associated algorithms for post-processing of measurements, the calculated resonance spectra presented here serve the purpose of simulating detector designs for the detection of explosives in the gas phase. In other words, for the detection of gas-phase explosives, these spectra can be assumed to provide a reasonable estimate of the dielectric response for purposes of the practical detection of explosives in gas phase. In addition, it must be remembered that many types of explosives existing in bulk should not be assumed to have microstructure or dielectric-response characteristics corresponding to a lattice. In many cases, explosives in bulk are characterized by clusters of molecules which are distributed within a host or binder material. For these cases, it is conceivable that many of the dielectric-response characteristics of isolated molecules could still be valid. This follows in that molecule-molecule coupling in these cases is expected to be more characteristic of isolated scattering sites, rather than that of a lattice structure.

With respect to more extensive DFT calculations concerning the ground-state absorption spectra of a bulk lattice or spectra corresponding to electronic-state transitions, it is important to note that the atomic positions of the relaxed or equilibrium configuration of a single isolated molecule, e.g., Tables 1, 3, 5, 7, and 9, provide a convenient starting point. Calculation of the dielectric response of a bulk system would entail, in principle, the construction of a super cell consisting of molecules initial positions of which are those determined using DFT for isolated systems. Additional constraints on this super cell could be based on crystallographic information concerning bulk density or lattice spacing. Calculation of the dielectric response associated with electronic-state transitions would entail the application of methods based on perturbation theory. In principle, for these methods, most of the computational effort is expended to be in the determination of the ground state, with respect to which all the excited states are determined self-consistently. These methods typically would be based on time-dependent density functional theory (DTDFT) (Ref 7).

9. Conclusion

The calculations of ground-state resonance structures associated with the high explosives β-HMX, PETN, RDX, TNT1, and TNT2 using DFT are intended to serve as reasonable estimates of molecular-level response characteristics, providing interpretation of dielectric-response features, intended for subsequent adjustment with additional knowledge of new experimental measurements and/or molecular structure and spectral theory.

Acknowledgment

This study is supported by the Office of Naval Research.

References

1. M.J. Frisch, G.W. Trucks, H.B. Schlegel, G.E. Scuseria, M.A. Robb, J.R. Cheeseman, G. Scalmani, V. Barone, B. Mennucci, G.A. Petersson, H. Nakatsuji, M. Caricato, X. Li, H.P. Hratchian, A.F. Izmaylov, J. Bloino, G. Zheng, J.L. Sonnenberg, M. Hada, M. Ehara, K. Toyota, R. Fukuda, J. Hasegawa, M. Ishida, T. Nakajima, Y. Honda, O. Kitao, H. Nakai, T. Vreven, J.A. Montgomery, Jr., J.E. Peralta, F. Ogliaro, M. Bearpark, J.J. Heyd, E. Brothers, K.N. Kudin, V.N. Staroverov, R. Kobayashi, J. Normand, K. Raghavachari, A. Rendell, J.C. Burant, S.S. Iyengar, J. Tomasi, M. Cossi, N. Rega, J.M. Millam, M. Klene, J.E. Knox, J.B. Cross, V. Bakken, C. Adamo, J. Jaramillo, R. Gomperts, R.E. Stratmann, O. Yazyev, A.J. Austin, R. Cammi, C. Pomelli, J.W. Ochterski, R.L. Martin, K. Morokuma, V.G. Zakrzewski, G.A. Voth, P. Salvador, J.J. Dannenberg, S. Dapprich, A.D. Daniels, Ö. Farkas, J.B. Foresman, J.V. Ortiz, J. Cioslowski, and D.J. Fox, *Gaussian 09, Revision A.1*, Gaussian, Inc., Wallingford, CT, 2009
2. A. Frisch, M.J. Frisch, F.R. Clemente, and G.W. Trucks, *Gaussian 09 User's Reference*, 2009, p 105–106
3. P. Hohenberg and W. Kohn, Inhomogeneous Electron Gas, *Phys. Rev.*, 1964, **136**, p B864
4. W. Kohn and L.J. Sham, Self-Consistent Equations Including Exchange and Correlation Effects, *Phys. Rev.*, 1965, **140**, p A1133
5. R.O. Jones and O. Gunnarsson, The Density Functional Formalism, Its Applications and Prospects, *Rev. Mod. Phys.*, 1989, **61**, p 689
6. W.W. Hager and H. Zhang., A survey of Nonlinear Conjugate Gradient Methods, *Pacific J. Optim.*, 2006, **2**, p 35–58
7. R.M. Martin, *Electronic Structures Basic Theory and Practical Methods*, Cambridge University Press, Cambridge, 2004, p 25
8. E.B. Wilson, J.C. Decius, and P.C. Cross, *Molecular Vibrations*, McGraw-Hill, New York, 1955
9. J.W. Ochterski, *Vibrational Analysis in Gaussian*, 1999, Available at http://www.gaussian.com/g_whitepap/vib.htm
10. J. Hooper, E. Mitchell, C. Konek, and J. Wilkinson, Terahertz Optical Properties of the High Explosive β-HMX, *Chem. Phys. Lett.*, 2009, **467**, p 309
11. C.A.D. Roeser and E. Mazur, Light-Matter Interactions on Femtosecond Time Scale *Frontiers of Optical Spectroscopy*, Vol 168, NATO Science Series, B. Di Bartolo and O. Forte, Ed., Kluwer Academic Publishers, Dordrecht, 2005, p 29
12. C.F. Bohren and D.R. Huffman, *Absorption and Scattering of Light by Small Particles*, Wiley-VCH Verlag, Weinheim, 2004
13. L.D. Landau, E.M. Lifshits, and L.P. Pitaevskii, *Physical Kinetics*, Butterworth-Heinemann, Oxford, 1981; and references therein
14. A.D. Becke, Density-functional Thermochemistry. III. The Role of Exact Exchange, *J. Chem. Phys.*, 1993, **98**, p 5648–5652
15. B. Miehlich, A. Savin, H. Stoll, and H. Preuss, Results of Obtained with the Correlation Energy Density Functionals of Becke and Lee, Yang and Parr, *Chem. Phys. Lett.*, 1989, **157**, p 200–206
16. A.D. McLean and G.S. Chandler, Contracted Gaussian-Basis Sets for Molecular Calculations. 1. 2nd Row Atoms, $Z = 11–18$, *J. Chem. Phys.*, 1980, **72**, p 5639–5648
17. T. Clark, J. Chandrasekhar, G.W. Spitznagel, and P.V.R. Schleyer, Efficient Diffuse Function-Augmented Basis-Sets for Anion Calculations. 3. The 3–21+G Basis Set for 1st-Row Elements Li-F, *J. Comput. Chem.*, 1983, **4**, p 294–301
18. M.J. Frisch, J.A. Pople, and J.S. Binkley, Self-Consistent Molecular Orbital Methods. 25. Supplementary Functions for Gaussian Basis Sets, *J. Chem. Phys.*, 1984, **80**, p 3265–3269